Diagnostic Efficacy of All Series of Dynamic Contrast Enhanced Breast MR Images Using Gradient Vector Flow (GVF) Segmentation and Novel Border Feature Extraction for Differentiation Between Malignant and Benign Breast Lesions

L. Bahreini MSc[1]
E. Fatemizadeh PhD[2]
M. Guity MD[3]

1. Department of Biomedical Engineering, Science and Research Branch, Islamic Azad University, Tehran, Iran.
2. Assistant Professor, Department of Biomedical Engineering, Science and Research Branch, Islamic Azad University, Tehran, Iran.
3. Associate Professor of Radiology, Advanced Diagnostic and Interventional Radiology Research Center (ADIR), Medical Imaging Center, Imam Khomeini Hospital, Tehran University of Medical Sciences, Tehran, Iran.

Corresponding Author:
Leila Bahreini
Address: 1st Golzar Aly., Adel Blvd., Babayi Blvd., Ponak Sq., Tehran, Iran.
PO. Box: 4515/775.
Tel: +9821 4447 4321
Fax: +9821 4447 4319
Email: leila.bahreini@gmail.com

Received July 13, 2010;
Revised September 7, 2010;
Accepted November 22, 2010.

Iran J Radiol 2010;7(4): 225-234

Background/Objective: To discriminate between malignant and benign breast lesions; conventionally, the first series of Breast Subtraction Dynamic Contrast-Enhanced Magnetic Resonance Imaging (BS DCE-MRI) images are used for quantitative analysis. In this study, we investigated whether using all series of these images could provide us with more diagnostic information.

Patients and Methods: This study included 60 histopathologically proven lesions. The steps of this study were as follows: selecting the regions of interest (ROI), segmentation using Gradient Vector Flow (GVF) snake for the first time, defining new feature sets, using artificial neural network (ANN) for optimal feature set selection, evaluation using receiver operating characteristic (ROC) analysis.

Results: The results showed GVF snake method correctly segmented 95.3% of breast lesion borders at the overlap threshold of 0.4. The first classifier which used the optimal feature set extracted only from the first series of BS DCE-MRI images achieved an area under the curve (AUC) of 0.82, specificity of 60% at sensitivity of 81%. The second classifier which used the same optimal feature set but was extracted from all five series of these images achieved an AUC of 0.90, specificity of 79% at sensitivity of 81%.

Conclusion: The result of GVF snake segmentation showed that it could make an accurate segmentation in the borders of breast lesions. According to this study, using all five series of BS DCE-MRI images could provide us with more diagnostic information about the breast lesion and could improve the performance of breast lesion classifiers in comparison with using the first series alone.

Keywords: BS DCE-MRI, GVF Snake Segmentation, Enhancement Sign, Fourier Factor, ROC Analysis

Introduction

Dynamic Contrast-Enhanced Magnetic Resonance Imaging (DCE-MRI) is an important imaging technique for the diagnosis of breast lesions. This system has been reported to have a high sensitivity in breast lesion diagnosis, whereas its specificity is variable.[1-8] The number of images acquired in MRI is much more than those acquired in conventional mammography or breast ultrasound, so their analysis would take a lot of time. It shows inter-observer variable as well.[9,10] All these problems make the development of breast MRI a big challenge in the recent years. Some efforts in different fields have been made for the development of breast MRI and

its processing. Breast lesion segmentation is one of the fields, in which such efforts have been made; Gihuijs et al.[11] and Gibbs et al.[12] performed the segmentation manually; Liney et al.[1] used a thresholding method; Chen et al.[13] and Meinel et al.[14] used a region growing method; Chen et al.[15-17] presented Fuzzy C-Means (FCM) segmentation and compared their results with the results of region growing, concluding that FCM segmentation is better than region growing; Ertaş et al.[18] employed cellular neural networks and 3D template matching for breast lesion segmentation.

Some other efforts have been made for feature extraction. Enhancement kinetics is a significant diagnostic feature which can strongly discriminate between malignant and benign lesions.[16,19] The reports showed that the texture features obtained from Gray Level Co-occurrence Matrix (GLCM) are the appropriate features.[12,17,20,21] Different morphological features have also been investigated and their results seem to be desirable.[1,14,20] Considering the fact that malignant tumors typically have irregular borders and shapes whereas benign masses have more round shapes with smooth and lobulated borders,[1,22] it seems that the features extracted from the border of the breast lesions would be able to differentiate between malignant and benign lesions. Accordingly, one of the objectives of this study was to find out some new effective features related to radial lengths.

Breast DCE-MRI images are acquired in different series (one pre-contrast series and several post-contrast series). While the first post-contrast series of DCE-MRI images is usually utilized in analysis, other post-contrast series would be probably informative. Another objective of this study was to investigate this issue.

It was also reported that Fourier Factor (FF) is a discriminative measure in conventional mammography images.[23] However, the efficiency of this measure in breast DCE-MRI images has not yet been investigated.[24] We decided to investigate the efficiency of FFs obtained using different signatures.

Centripetal enhancement and centrifugal enhancement are two specific signs. Another objective of this study was to define two features for diagnosis of these two signs.

This study consisted of the following mentioned stages; selecting the regions of interest (ROIs), segmentation using Gradient Vector Flow (GVF) snake for the first time, defining three new feature sets, using artificial neural network (ANN) for optimal feature set selection, efficacy evaluation of diagnostic classifiers using receiver operating characteristic (ROC) analysis.

Materials and Methods

The image database of this study has been collected under a standard protocol including one pre-contrast and five post-contrast series. In this study, we used a 1.5 Tesla MRI system which has a dedicated bipolar phased-array breast coil (GE Healthcare, Milwaukee, WI, USA). The breast DCE-MRI was performed using T1-weighted 3D spoiled gradient-recalled echo pulse sequence with these characteristics: echo time=4.2 ms, repetition time=9 ms, flip angel= 30°, FOV=32-40 cm and matrix size= 512×512. The temporal resolution of each dynamic acquisition series was 80 seconds. In each series of images, we had an average of 64 axial slices (depending on the thickness of the breast). These slices have the thickness of 4 mm. The first (pre-contrast) series was acquired before the injection of contrast agent. Then 0.2 mmol/kg of Gd-DTPA was injected manually and intravenously followed by 20cc normal saline. After the injection of contrast agent, five post-contrast breast imaging series were acquired. This study included 60 histopathologically proven lesions (38 malignant and 22 benign). Table 1 shows the pathology of all analyzed lesions. The process of this study was approved by the ethics committee.

Pre-processing

In this study, breast subtraction DCE-MRI (BS DCE-MRI) images were used. These subtraction images were obtained by subtracting the pre-contrast series from each five post-contrast series of images. Therefore, there were five series of BS DCE-MRI images for each patient.

For each lesion, the operator selected a representative image slice for each five series of BS DCE-MRI images. The characteristic of these representative images was that they showed the best appearance of the lesion among other image slices. These representative image slices had the same number in each series. Then, the operator placed the same rectangular boxes in them, indicating the suspicious location of the lesion. These five rectangular boxes were treated as the regions of interest (ROIs) for each lesion. Figure 1 shows an example of selecting ROIs in five representative image slices of the lesion which were selected by the operator.

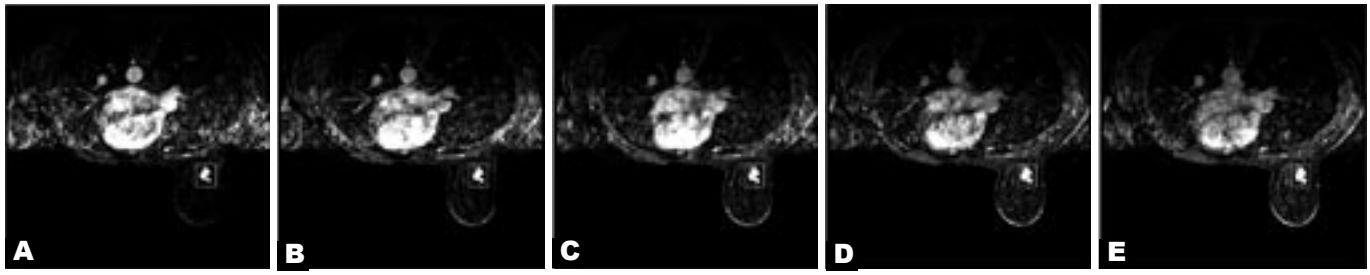

Fig. 1. Example of selecting same ROIs for the breast lesion in: **A.** First, **B.** Second, **C.** Third, **D.** Fourth and **E.** Fifth representative image slices.

Segmentation

As we are looking for the quantitative evaluation of the features extracted from the lesion borders in this study, it seems necessary to employ an edge-based segmentation method in order to make an accurate segmentation in the borders of the breast lesions. To accomplish this purpose, we followed the parametric active contour methods. Through these methods, considering the appearance characteristics of BS DCE-MRI images and the result of different parametric active contour segmentation methods,[25] we chose GVF snake method which was developed by Xu and Prince.[26]

GVF Snake in Breast Lesion Segmentation

In this study, GVF snake method was used for breast lesion segmentation in the different series of BS DCE-MRI images through the following stages:[27]

1- First, an initial contour was drawn in the ROI by the operator, which surrounded the whole lesion.

2- In the next stage, the edge map of ROI was calculated according to equation 1 in the appendix with a determined σ whereas I (x,y) was ROI.[26-28]

3- Then the GVF external force was calculated from the edge map and with the setting of two parameters: regularization parameter μ and GVF iteration number N, according to the GVF vector field that was obtained from solving the Euler equation represented in equation 2 (see the appendix).[26,27,29]

4- Finally, GVF snake deformation was performed according to GVF snake obtained from solving equation 3 in the appendix which contains these parameters: elasticity α, rigidity β, viscosity γ, external force factor X, and deformation steps (DS).[26,27,30]

After finishing the predefined DS for GVF snake deformation, the final contour was obtained.[27] The above mentioned segmentation method was employed for each lesion in its five representative image slices. For implementing this segmentation method, we used a computer program written in MATLAB.[31] Segmentation of each image typically took less than six seconds on a laptop with 1.86 GHZ Intel Core™ Dou Processor (Fig. 2). Figure 2B shows the initial contour selection of a lesion in its five representative image slices and Figure 2C shows the corresponding results of GVF snake segmentation method.

The values of GVF snake parameters used for the breast lesion segmentation of this study are presented in Table 2.

The values of α and β were chosen small in order to develop the contour to the corners. γ was chosen bigger than α and β in order to have a smooth contour

Table 1. Histopathology of Malignant and Benign Breast Lesions

Type of Tumors	Number	Percentage
Malignant Lesions:	38	
Invasive Ductal Carcinoma	19	50%
Invasive Lobular Carcinoma	8	21%
Ductal Carcinoma In-Situ	7	18.5%
Others	4	10.5%
Benign Lesions:	22	
Fibroadenoma	14	63.6%
Fibrocystic Changes	5	22.8%
Others	3	13.6%

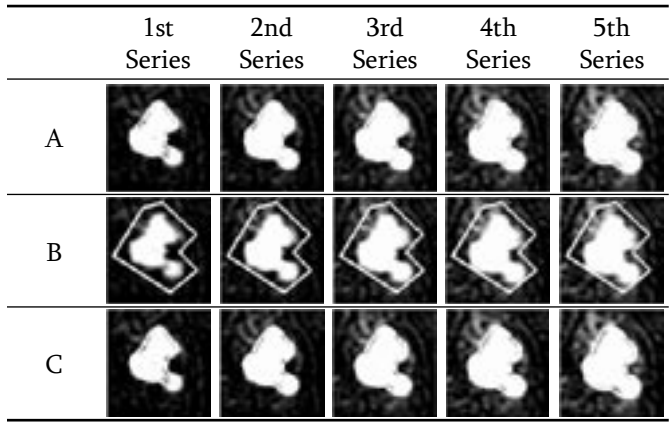

Fig. 2. Example of lesion border segmentation in five representative image slices.
A. Lesion border segmentation by an expert radiologist.
B. Initial contour selection.
C. Lesion border segmentation by GVF snake.

Table 2. Values of GVF Snake Parameters

Parameter	Value
σ	0.25-0.75
μ	0.1-0.2
N	80-200
α	0.05-0.1
β	0-0.07
γ	1-1.4
X	0.6-1.7
DS	10-200

α: Elasticity, β: Rigidity, γ: Viscosity, σ: Standard deviation of Gaussian, DS: Deformation Steps, μ: Regularization parameter, N:GVF iteration number, X:External force factor.

in the boundaries. X was selected in a way that the contour stopped at the edges of the lesion. μ and N were chosen relative to the presence of noise in the image. The number of DS was considered in a way that the appropriate final contour was obtained. [25,27]

Feature Extraction

In this section, some feature sets, introduced to investigate in five series of BS DCE-MRI images. The first feature set was related to the radial length. Radial length (r) is defined as the Euclidean distance between each contour point and the center of the contour. [14,20] In this stage, we extracted the mean, spiculation (which is defined as the standard deviation (SD) of radial length), and the entropy of radial length which were reported discriminative in previous studies.[14,20] Some new features related to radial length are introduced in this study including: variance of radial length, variance to mean ratio (V to M), mean to variance ratio (M to V), RL ratio, RL ratio inversion (see the appendix). The next feature of this set was defined as the Maximum Diameter (MD) of the lesion.[1]

The efficiency of FF in breast DCE-MRI images has not been investigated yet.[24] So, the next feature set was the FFs. To obtain the FFs, we need to take the following steps:

1. Contour Signature

Contour signature is an important part in the definition of FD. It reduces 2D Contour boundary to 1D function so that it facilitates the process of obtaining invariant shape feature by the use of Fourier transform.[32] The signatures used in this study were as below:

1.1. Radial Distance (RD): this signature is defined as the Euclidean distance between boundary contour points and its centroid.[14,32]

1.2. Farthest Point Distance (FPD): this signature, like human visual system, attends to contour corners. It is defined as the Euclidean distance between each boundary contour point and the farthest point to that.[32]

1.3. Complex Coordinates (CC): this signature is obtained by treating each boundary contour point as a complex number.[32]

1.4. Polar Coordinates (PC): this signature is defined using radial distance signature and polar angle signature (θ(n)). It has been proved that all these signatures are translation invariant.[32]

2. Fourier Descriptor (FD)

FD is a powerful technique which provides us with interesting characteristics such as translational, scale and rotational invariance.[32] The reason of using FD is to introduce Fourier transformed boundary as a shape feature.[33] Shape FD is defined using discrete Fourier transformation of a signature Z(n) in the appendix.[32]

The rotation invariance of FDs was obtained by considering the magnitude of FDs and ignoring their phase information.[32] The scale invariance of FDs for the real-valued and complex-valued signatures was represented in the appendix.[32] The translation invariance of FDs was provided by translation invariance of signatures.[32]

3. Fourier Factor (FF)

FF, defined in the appendix,[34] measures the presence of high frequency components and roughness in the contour.[33,34] FF has some advantages; it is always in the range of [0,1], and is invariant to starting point, contour size, translation and rotation. It is also insensitive to noise. The increase in the complexity and roughness of the contour results in an increase in FF values. That is why we expect larger FF values for malignant lesions which have more complex and rough contours and smaller FF values for benign lesions which have simpler contours.[23,33,34]

Statistical analyses of the extracted features for the benign and malignant groups were performed using an independent samples t-test with either a pooled or separate variance as determined by the Levene's test for equality of variances.[1]

The next feature set was defined for diagnosis of centripetal enhancement and centrifugal enhancement signs.

Defining Feature for Centripetal Enhancement Sign Diagnosis

In these signs, peripheral ring enhancement occurs first, then it spreads toward the center of the mass within time.[35] This feature was defined as the decrease of the internal contour perimeters of the lesions from the first to the fifth series of BS DCE-MRI images.

Defining Feature for Centrifugal Enhancement Sign Diagnosis

In this sign, in contrast to centripetal enhancement, the enhancement is initially more pronounced at the center of the mass and spreads to the boundaries.[35] This feature was defined as the increase of the external contour perimeters of the lesions from the first to the fifth series.

Diagnostic Feature Selection Using Artificial Neural Network (ANN)

After GVF Snake Segmentation and obtaining the final contours of each lesion in its five representative image slices, the mentioned features were extracted. Then ANN was utilized to achieve an optimal feature set which differentiates between malignant and benign lesions.

To obtain the optimal feature set, each feature extracted from the first series of BS DCE-MRI images (first representative image slice of each lesion) has been normalized to have zero mean and unit variance. The Multiple Layer Perceptron (MLP) topology with three layers was used.[14,20,36] The best structure of MLP was determined by selecting the one which leads to the best performance as follows: the input layer and the hidden layer had five nodes each. The output layer contained one node. The transfer function of the hidden layer nodes was hyperbolic tangent sigmoid and the transfer function of the output layer node was Log-sigmoid. The output values ranged from zero to one which indicated the level of malignancy, where zero means absolutely benign and one means absolutely malignant. For training, Levenberg-Marquardt back-propagation was used and the network performance was evaluated using root mean square error. In the training stage, the criteria for convergence were set to a root mean squared error<0.0001 or the maximum iteration of 600. The whole data set was utilized in training stage using leave-one-out cross validation. Feature selection was performed to find the optimal diagnostic performance to classify features extracted from the first series of BS DCE-MRI images. During training, the network output was compared to the biopsy results as target in order to find the optimal feature set. It was chosen by a number of trial-and-error runs so that the trained classifier produced the least square rate.

Another objective of this study was to investigate whether using all series of DCE-MRI images improves the differentiating capability between malignant and benign lesions compared to using only the first series; therefore another ANN classifier with the mentioned topology was applied. In contrast to the first classifier, the second classifier used the normalized features extracted from all series of BS DCE-MRI images (five representative image slices of each lesion) as input. The training stage of the second classifier was performed the same as the first classifier. Then the performance of these two classifiers was evaluated using receiver operating characteristics (ROC) curve analysis.

Results

Evaluation of GVF Snake Segmentation Method

In this study, for the first time, the GVF Snake Segmentation Method was used for breast lesion segmentation in BS DCE-MRI images. An expert radiologist manually determined the breast lesion borders in all five representative image slices. These results were assumed as "ground truth". Figure 2A shows the "ground truth" selection of a lesion in its 5 representative image slices. To compare the result of the computerized segmentation with the "ground truth", we used the overlap measure as follows:[15]

$$O=\frac{(C\cap R)}{(C\cup R)} \quad [20]$$

Where C is the set of boundary pixels obtained from the computerized segmentation and R is the set of boundary pixels manually determined by the radiologist. To compare the segmentation results of GVF snake method with FCM method, all the breast lesions were also segmented using FCM method.[15-17] The results showed the GVF snake segmentation method correctly segmented 97.4% of the malignant lesion borders and 91.8% of the benign lesion borders in five series of BS DCE-MRI images at the overlap threshold of 0.4, whereas the FCM method correctly segmented 91.6% of the malignant lesion borders and 81% of the

Table 3. Results of Some Features Extracted from All Five Series of BS DCE-MRI Images

Mean ± SD			
Feature	Malignant	Benign	P Value
Var	6.67±5.44	1.24±0.90	0.007
SD	2.35±1.54	1.06±0.35	0.03
V to M	0.567±0.378	0.265±0.129	0.05
Circularity	0.24±0.07	0.23±0.08	0.5
M to V	2.78±1.84	4.70±2.10	0.07
Sphericity	4.50±1.62	4.87±1.37	0.6
FF_{CC}	0.362±0.059	0.295±0.012	0.02
FF_{PC}	0.711±0.051	0.662±0.053	0.05
FF_{RD}	0.667±0.065	0.645±0.043	0.3
FF_{FPD}	0.670±0.060	0.616±0.060	0.09

Var: Variance of radial length, SD: Standard Deviation of radial length, V to M: Variance to Mean ratio of radial length, M to V: Mean to Variance ratio of radial length, FF_{CC}: Fourier Factor obtained using Complex Coordinates signature, FF_{PC}: Fourier Factor obtained using Polar Coordinates signature, FF_{RD}: Fourier Factor obtained using Radial Distance signature, FF_{FPD}: Fourier Factor obtained using Farthest Point Distance signature.

benign lesion borders.

Table 3 shows the result of some extracted features. This table contains the mean and the standard deviation (mean±SD) values of these features for malignant and benign groups extracted from all five series of BS DCE-MRI images. The result showed Variance, SD, V to M, FF_{CC} and FF_{PC}were discriminative between malignant and benign lesions, while their p values were lower than 0.05.

Results of the Defined Feature for Centripetal Enhancement Sign Diagnosis

The defined feature has been investigated on three cases with centripetal enhancement sign. In all three cases, there was a decrease in the internal contour perimeters of the lesions from the first to the fifth series of BS DCE-MRI images. The diagnosis of this sign can guide to carcinoma.[35]

Results of the Defined Feature for Centrifugal Enhancement Sign Diagnosis

The defined feature has been investigated on two cases with centrifugal enhancement sign. In both cases, there was an increase in the external contour perimeters of the lesion from the first to the fifth series. However, after the calculation, this feature was confirmed by the radiologist because some lesions with this feature did not necessarily have this kind of sign. Diagnosis of this sign can guide to benign lesion.[35]

Table 4. Results of the Two Defined Features for Centripetal and Centrifugal Enhancement Sign Diagnosis Which are Related to Figs. 2A&B, Respectively

Perimeter(mm)						
Sign	1st Series	2nd Series	3rd Series	4th Series	5th Series	Changing
Centripetal Enhancement	86.14	81.42	79.06	75.52	74.34	Decreasing
Centrifugal Enhancement	56.64	60.18	61.36	62.54	64.90	Increasing

Figure 3 shows a lesion which has centripetal enhancement/centrifugal enhancement sign in its 5 representative image slices with their internal contours/external contours. In Table 4, the internal contour /external contour perimeters of the lesion shown in Figure 3 are observed.

Performance Evaluation of the First ANN Classifier

When we used the mentioned features of this study, the first classifier selected by ANN included five features: Entropy and Variance of radial length, RL Ratio, MD, and FF_{CC} as the optimal feature set extracted only from the first series of BS DCE-MRI images. Using these five features for ROC analysis, the first ANN classifier achieved an area under the curve (AUC) of 0.82. At sensitivity of 81%, this classifier reached the specificity of 60% (95% confidence interval: 73-92).

Performance Evaluation of the Second ANN Classifier

The second classifier selected by ANN included five features (the same as the first classifier): Entropy and

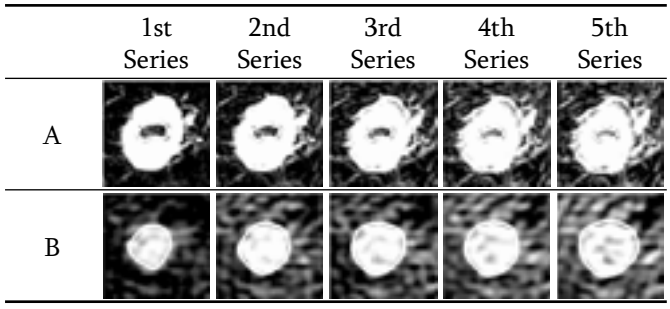

Fig. 3. Example of lesions which have **A.** Centripetal and **B.** Centrifugal enhancement signs in five representative image slices with their internal and external contours, respectively.

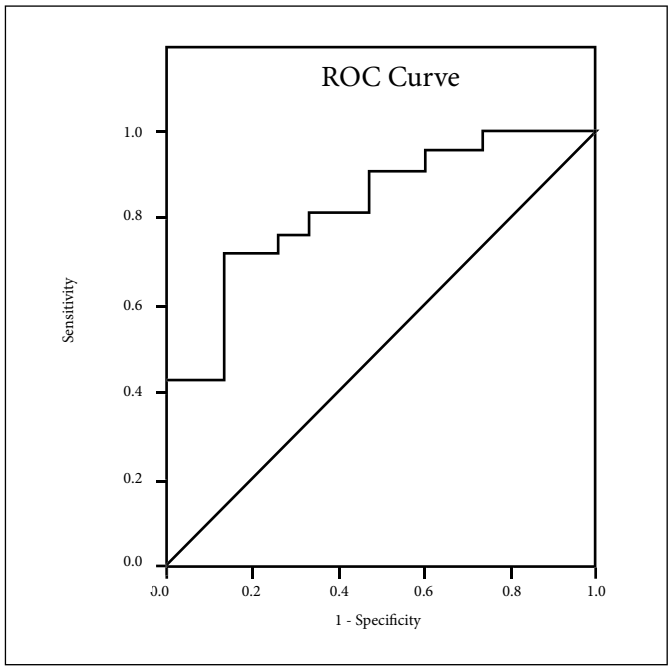

Fig. 4. The receiver operating characteristic curve for the first ANN classifier which used the optimal feature set extracted only from the first series of BS DCE-MRI images. The area under the curve is 0.82.

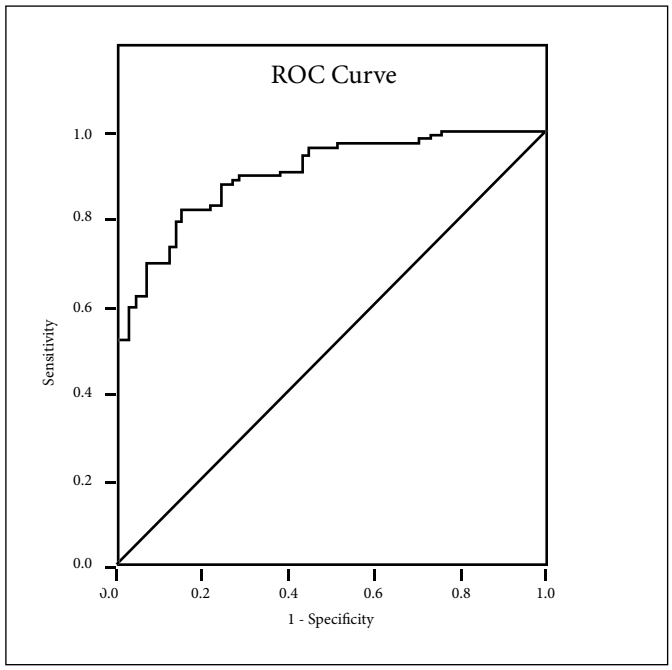

Fig. 5. The receiver operating characteristic curve for the second ANN classifier which used the optimal feature set extracted from all five series of BS DCE-MRI images. The area under the curve is 0.90.

Variance of radial length, RL Ratio, MD, and FF_{CC} as the optimal feature set extracted from all five series of BS DCE-MRI images. Using these five features for ROC analysis, the second ANN classifier achieved AUC of 0.90. At sensitivity of 81%, this classifier reached the specificity of 79% (95% confidence interval 86-94). Figures 4 and 5 show the ROC curve for the first/second ANN classifier and table 5 shows the ROC curve statistics of these classifiers. Tables 6 and 7 show the (mean±SD) values of RL Ratio, MD, and FF_{CC} for malignant and benign groups extracted from the first/all five series.

Discussion

In recent years, the development of the computer-aided diagnosis (CAD) for breast MRI has been a great challenge. Some investigations have pursued breast lesion segmentation, feature extraction from breast lesion, and diagnostic classification.[1,11-21,36]

Table 5. ROC Analysis Statistics of a. the First ANN Classifier Which Used the Optimal Feature Set Extracted Only from First Series of BS DCE-MRI Images, b. the Second ANN Classifier Which Used the Optimal Feature Set Extracted from All Five Series of BS DCE-MRI Images

ANNs	AUC	Sensitivity	Specificity	95% CI
First Classifier	0.82	81%	60%	73-92
Second Classifier	0.90	81%	79%	86-94

AUC: area under the receiver operating characteristic curve, CI: confidence interval

In this study, for the first time, an edge-based segmentation method named GVF snake was used for breast lesion segmentation. So far, most lesion segmentations have been done manually or by using semi-automated/automated segmentation methods based on pixel intensity.[1,11-18] In this study, the GVF snake method was used which is edge-based and uses the knowledge of radiologists for initial contour selection. This method is a powerful parametric active contour method in locating the object boundary that can develop to corners and form smooth contours.[25,26] This method, used for other medical image segmentation, has been reported satisfactory.[25] The results showed GVF snake method correctly segmented 95.3% of breast lesion borders at the overlap threshold of 0.4, whereas FCM method correctly segmented 87.7% of them. Furthermore, the GVF snake method resulted in a unified region whereas FCM method sometimes resulted incorrectly in some disconnected regions for segmenting a lesion. The result of GVF snake method showed some lesions were not correctly segmented because in some cases the surrounding tissue was enhanced which made the detection of the lesion borders more difficult. In addition, some benign lesions had low enhancement or ill-defined margin which also made the detection of lesion borders more difficult.

Table 6. Results of Some Optimal Features Extracted Only from First Series of BS DCE-MRI Images

	Mean ± SD		
Feature	Malignant	Benign	P Value
RLR	25.8±18.3	6.1±4.2	0.02
MD	27.0±9.7	13.4±5.0	0.007
FF_{CC}	0.349±0.034	0.308±0.016	0.02

RLR: Radial Length Ratio, MD: Maximum Diameter, FF_{CC}: Fourier factor obtained using complex coordinates signature

Table 7. Results of Some Optimal Features Extracted from All Five Series of BS DCE-MRI Images

	Mean ± SD		
Feature	Malignant	Benign	P Value
RLR	30.2±22.1	6.0±3.9	0.01
MD	29.4±12.3	13.4±4.3	0.005
FF_{CC}	0.362±0.059	0.295±0.012	0.02

RLR: Radial Length Ratio, MD: Maximum Diameter, FF_{CC}: Fourier factor obtained using complex coordinates signature

The primary results of this study in all series of BS DCE-MRI images showed:

The Variance of radial length compared to the SD of radial length, V to M compared to circularity, and M to V compared to sphericity were more efficient in discrimination. Entropy, Variance, SD, V to M, MD and RL Ratio were discriminative between malignant and benign lesions, while their p values were lower than 0.05. Circularity and sphericity were not discriminative as reported in previous studies.[1,20] According to the results, all the radial length related features had higher mean values in malignant groups than in benign ones except for M to V and sphericity.

Extracting FFs obtained using different contour signatures was not previously investigated in breast MRI. The results showed the FFs obtained using complex-valued signatures (FF_{CC} and FF_{PC}) are more efficient compared to FFs obtained using real-valued signatures (FF_{RD} and FF_{FPD}), while their p values were lower than 0.05. Among FFs, $FF_{CC}$was more discriminative as it also was reported in X-ray mammography.[23,33]

The two defined features for diagnosis of centripetal and centrifugal enhancement signs were capable of detecting them. Diagnosis of the first one can guide to carcinoma and diagnosis of the second one can guide to benign lesion.[35]

Comparing Tables 6 and 7, it is concluded that the p values of RL Ratio, MD, and FF_{CC}, extracted from all five series of BS DCE-MRI images were lower than the p values of these features extracted only from the first series. It is concluded that these features were more discriminative when extracted from all five series.

The ANN was used to find the optimal feature set which had resulted in the best performance in classification into malignant and benign groups.[14,20,36] In this study, a three layer MLP was used which was limited to five nodes in hidden layer to avoid overtraining. For training, the whole data set was utilized using the leave-one-out cross validation. The optimal feature set included: Entropy and variance of radial length, RL Ratio, MD and FF_{CC}. As reported previously, entropy and FF_{CC} were obtained efficient.[14,23,33,36]

Results showed that the first classifier which used the optimal feature set extracted only from the first series achieved an AUC of 0.82 whereas this value for the second classifier which used the same optimal feature set but was extracted from all five series was 0.90. This increase in AUC values indicated the better performance of the second classifier. This result also showed that in addition to the first series of images which is usually used for quantitative analysis, other series of these images have diagnostic information. As the results showed, the first classifier at sensitivity of 81% reached the specificity of 60% and the second classifier reached the specificity of 79% at the same sensitivity. The increase in both AUC values and the specificity at the sensitivity of 81% showed using all five series of the images could provide us with more diagnostic information about the lesion in comparison to the using of the first series alone. And this increase of specificity at the same high sensitivity indicated the decrease of false positive rate which could be translated into fewer unnecessary biopsies and follow-up imaging studies.

References

1. Liney GP, Sreenvias M, Gibbs P, Garcia-Alvarez R, Turnbull LW. Breast lesion analysis of shape technique: semiautomated vs. manual morphological description. J Magn Reson Imaging 2006 Apr;23(4):493-8.
2. Starita A, LaManna S, Majidi D, Caramella D, Cilotti A. Magnetic resonance in mammography: a quantitative evaluation tool of contrast-enhanced magnetic resonance of the breast. In: Institution of Electrical Engineers, Institute of Physics (Great Britain), British

Medical Informatics Society, European Conference on Artificial Intelligence in Medicine. First international conference on advances in medical signal and information processing. Piscataway, NJ: Institute of Electrical and Electronics Engineers; 2000. p. 200-5.
3. Mumtaz H, Hall-Craggs MA, Davidson T, Walmsley K, Thurell W, Kissin MW et al. Staging of symptomatic primary breast cancer with MR imaging. AJR Am J Roentgenol 1997 Aug;169(2):417-24.
4. Fischer U, Kopka L, Grabbe E. Breast carcinoma: effect of preoperative contrast-enhanced MR imaging on the therapeutic approach. Radiology 1999 Dec;213(3):881-8.
5. Esserman L, Hylton N, Yassa L, Barclay J, Frankel S, Sickles E. Utility of magnetic resonance imaging in the management of breast cancer: evidence for improved preoperative staging. J Clin Oncol 1999 Jan;17(1):110-9.
6. Zhang Y, Fukatsu H, Naganawa S, Satake H, Sato Y, Ohiwa M et al. The role of contrast-enhanced MR mammography for determining candidates for breast conservation surgery. Breast Cancer 2002;9(3):231-9.
7. Rieber A, Schirrmeister H, Gabelmann A, Nuessle K, Reske SN, Kreienberg R et al. Pre-operative staging of invasive breast cancer with MR mammography and/or PET: boon or bunk? Br J Radiol 2002 Oct;75(898):789-98.
8. Schelfout K, Van GM, Kersschot E, Colpaert C, Schelfhout AM, Leyman P et al. Contrast-enhanced MR imaging of breast lesions and effect on treatment. Eur J Surg Oncol 2004 Jun;30(5):501-7.
9. Wedegartner U, Bick U, Wortler K, Rummeny E, Bongartz G. Differentiation between benign and malignant findings on MR-mammography: usefulness of morphological criteria. Eur Radiol 2001;11(9):1645-50.
10. Mussurakis S, Buckley DL, Coady AM, Turnbull LW, Horsman A. Observer variability in the interpretation of contrast enhanced MRI of the breast. Br J Radiol 1996 Nov;69(827):1009-16.
11. Gilhuijs KG, Giger ML, Bick U. Computerized analysis of breast lesions in three dimensions using dynamic magnetic-resonance imaging. Med Phys 1998 Sep;25(9):1647-54.
12. Gibbs P, Turnbull LW. Textural analysis of contrast-enhanced MR images of the breast. Magn Reson Med 2003 Jul;50(1):92-8.
13. Chen W, Giger ML, Lan L, Bick U. Computerized interpretation of breast MRI: investigation of enhancement-variance dynamics. Med Phys 2004 May;31(5):1076-82.
14. Meinel LA, Stolpen AH, Berbaum KS, Fajardo LL, Reinhardt JM. Breast MRI lesion classification: improved performance of human readers with a back propagation neural network computer-aided diagnosis (CAD) system. J Magn Reson Imaging 2007 Jan;25(1):89-95.
15. Chen W, Giger ML, Bick U. A fuzzy c-means (FCM)-based approach for computerized segmentation of breast lesions in dynamic contrast enhanced MR images. Acad Radiol 2006 Jan;13(1):63-72.
16. Chen W, Giger ML, Bick U, Newstead GM. Automatic identification and classification of characteristic kinetic curves of breast lesions on DCE-MRI. Med Phys 2006 Aug;33(8):2878-87.
17. Chen W, Giger ML, Li H, Bick U, Newstead GM. Volumetric texture analysis of breast lesions on contrast-enhanced magnetic resonance images. Magn Reson Med 2007 Sep;58(3):562-71.
18. Ertaş G, GülÇür HÖ, Osman O, Uçan ON, Tunaci M, Dursun M. Breast MR segmentation and lesion detection with cellular neural networks and 3D template matching. Comput Biol Med 2008 Jan;38(1):116-26.
19. Kuhl CK, Mielcareck P, Klaschik S, Leutner C, Wardelmann E, Gieseke et al. Dynamic breast MR imaging: are signal intensity time course data useful for differential diagnosis of enhancing lesions? Radiology 1999 Apr;211(1):101-10.
20. Nie K, Chen JH, Yu HJ, Chu Y, Nalcioglu O, Su MY. Quantitative analysis of lesion morphology and texture features for diagnostic prediction in breast MRI. Acad Radiol 2008 Dec;15(12):1513-25.
21. Woods BJ, Clymer BD, Kurc T, Heverhagen JT, Stevens R, Orsdemir A et al. Malignant-lesion segmentation using 4D co-occurrence texture analysis applied to dynamic contrast-enhanced magnetic resonance breast image data. J Magn Reson Imaging 2007 Mar;25(3):495-501.
22. Kuhl CK. MRI of breast tumors. Eur Radiol 2000;10(1):46-58.
23. Rangayyan RM, El-Faramawy NM, Desautels JEL, Alim OA. Measures of acutance and shape for classification of breast tumors. IEEE Trans Med Imaging 1997 Dec;16(6):799-810.
24. Behrens S, Laue H, Althaus M, Boehler T, Kuemmerlen B, Hahn HK et al. Computer assistance for MR based diagnosis of breast cancer: present and future challenges. Comput Med Imaging Graph 2007 Jun-Jul;31(4-5):236-47.
25. He L, Peng Z, Everding B, Wang X, Han CY, Weiss KL et al. A comparative study of deformable contour methods on medical image segmentation. Image Vis Comput 2008;26(2):141-63.
26. Xu C, Prince JL. Snakes, shapes, and gradient vector flow. IEEE Trans Image Process 1998;7(3):359-69.
27. Bahreini L, Fatemizadeh E, Gity M. Gradient vector flow snake segmentation of breast lesions in dynamic contrast-enhanced MR images. The 17th Iranian Conference on Biomedical Engineering (ICBME), 2010 Nov 3-4; Isfahan, Iran.
28. Jain AK. Fundamentals of digital image processing. Englewood Cliffs, NJ: Prentice-Hall; 1989.
29. Courant R, Hilbert D. Methods of mathematical physics. vol 1. New York: Interscience; 1953.
30. Kass M, Witkin A, Terzopoulos D. Snakes: active contour models. Int J Comput Vis 1987;1:321-31.
31. Xu Ch, Prince Jerry L. Active contours, deformable models, and gradient vector flow. Available at: http://iacl.ece.jhu.edu/projects/gvf/. Accessed May 2, 2009.
32. El-ghazal A, Basir O, Belkasim S. Farthest point distance: a new shape signature for Fourier descriptors. Signal Process Image Comm 2009 Aug;24(7):572-86.
33. Rangayyan RM, Nguyen TM. Fractal analysis of contours of breast masses in mammograms. J Digit Imaging 2007 Sep;20(3):223-37.
34. Shen L, Rangayyan RM, Desautels JEL. Detection and classification of mammographic calcifications. Int J Pattern Recogn Artif Intell 1993;7(6):1403-16.
35. Kaiser WA. Signs in MR-Mammography. Germany, Springer Berlin Heidelberg New York, 2008.
36. McLaren CE, Chen WP, Nie K, SU MY. Prediction of malignant breast lesion from MRI features: A comparison of artificial neural network and logistic regression techniques. Acad Radiol 2009 Jul;16(7):842-51.

Appendix:

Segmentation Equations:

$f(x,y)=|\nabla[G_\sigma (x,y) * I(x,y)\ ]\ |$ Equation 1[26-28]

$\mu\nabla^2 u-(u-f_x)(f_x^2+f_y^2)=0$ Equation 2[26,27,29]

$\mu\nabla^2 v-(v-f_y)(f_x^2+f_y^2)=0$

$X_t (s,t)=\alpha X''(s,t)-\beta X''''(s,t)+V$ Equation 3

Features:

Variance: $Var=(1/n)\sum_{i=1}^{n}(r_i-M)^2$

Variance to Mean ratio(V to M): $VtM=Var/M$

Mean to Variance ratio (M to V): $MtV=M/Var$

RL Ratio: $RLR=\frac{(\sum_{i=1}^{n}|r_i-M|)^2}{(n\times M)}$

RL Ratio Inversion: $RLRI=\frac{(n\times M)}{(\sum_{i=1}^{n}|r_i-M|)^2}$

In which n is the number of radial lengths *(i=1,2,…,n)* and M is the mean value of them.

Fourier Descriptor: $FD_k=\frac{1}{N}\sum_{n=0}^{N-1}Z(n)e^{-j\frac{2\pi}{N}nk}$

$n=0,1,....N-1,\ k=-\frac{N}{2},...,-1,0,1,2,...,\frac{N}{2}-1$

Fourier Factor: $FF=1-\frac{\sum_{k=-N/2+1}^{N/2}F_{normalized}}{\sum_{k=-N/2+1}^{N/2}F_{normalized}}$

In which $F_{normalized}$ for real-valued signature is obtained as follows:

$$F_{normalized}=\begin{cases}0 & k=0\\ F_{normal\text{-}real} & Otherwise\end{cases}$$

$$F_{normal\text{-}real}=[\frac{|FD_1|}{|FD_0|},\frac{|FD_2|}{|FD_0|},...,\frac{|FD_{N/2}|}{|FD_0|}\ ]$$

And for complex-valued signature:

$$F_{normalized}=\begin{cases}0 & k=0\\ F_{normal\text{-}complex} & Otherwise\end{cases}$$

$$F_{normal\text{-}complex}=[\frac{|FD_{-N/2}|}{|FD_1|},...,\frac{|FD_{-1}|}{|FD_1|},\frac{|FD_0|}{|FD_1|},\frac{|FD_2|}{|FD_1|},...,\frac{|FD_{N/2-1}|}{|FD_1|}\ ]$$